JACS
JOURNAL OF THE AMERICAN CHEMICAL SOCIETY
Article
pubs.acs.org/JACS

Charge-Dependent Dynamics of a Polyelectrolyte Dendrimer and Its Correlation with Invasive Water

Bin Wu,[†,#,‡] Yun Liu,*[,∇,○] Xin Li,[†] Eugene Mamontov,[§] Alexander I. Kolesnikov,[§] Souleymane O. Diallo,[∥] Changwoo Do,[†] Lionel Porcar,[◆] Kunlun Hong,[‡] Sean C. Smith,[‡] Li Liu,[#] Gregory S. Smith,[†] Takeshi Egami,[⊥,¶] and Wei-Ren Chen*[,†]

[†]Biology and Soft Matter Division, [‡]The Center for Nanophase Materials Sciences, [§]Chemical & Engineering Materials Division, [∥]Quantum Condensed Matter Division, and [⊥]Joint Institute for Neutron Sciences, Oak Ridge National Laboratory, Oak Ridge, Tennessee 37831, United States

[#]Department of Mechanical, Aerospace & Nuclear Engineering, Rensselaer Polytechnic Institute, Troy, New York 12180, United States

[∇]The NIST Center for Neutron Research, National Institute of Standards and Technology, Gaithersburg, Maryland 20899-6100, United States

[○]Department of Chemical Engineering, University of Delaware, Newark, Delaware 19716, United States

[◆]Institut Laue-Langevin, B.P. 156, F-38042 Grenoble CEDEX 9, France

[¶]Department of Materials Science and Engineering and Department of Physics and Astronomy, The University of Tennessee, Knoxville, Tennessee 37996-1508, United States

ABSTRACT: Atomistic molecular dynamics (MD) simulations were carried out to investigate the local dynamics of polyelectrolyte dendrimers dissolved in deuterium oxide (D_2O) and its dependence on molecular charge. Enhanced segmental dynamics upon increase in molecular charge is observed, consistent with quasielastic neutron scattering (QENS) measurements. A strong coupling between the intradendrimer local hydration level and segmental dynamics is also revealed. Compelling evidence shows these findings originate from the electrostatic interaction between the hydrocarbon components of a dendrimer and the invasive water. This combined study provides fundamental insight into the dynamics of charged polyelectrolytes and the solvating water molecules.

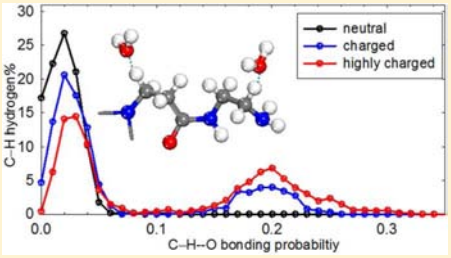

1. INTRODUCTION

Polyelectrolyte dendrimers are charged, branched macromolecules soluble in aqueous solutions. They are fascinating from a theoretical viewpoint due to the complexity arising from the polymeric structure with colloid-like globular shape and long-ranged Coulombic interactions.[1] They are well-controlled, monodisperse molecules with a tunable charge. Many of their proposed applications add to their scientific importance.[2,3] Consequently, they have been the subject of many ongoing research projects.

The questions of what is the equilibrium structure of a single dendrimer in solution and what is its dependence on molecular charge have been the subject of extensive theoretical,[4] computational,[5] and experimental[6] investigations. Contrast variation small angle neutron scattering (CVSANS)[7] and molecular dynamics (MD)[1,5,8] studies concluded that due to the backfolding of hydrocarbon components of dendrimer,[9] the intradendrimer mass distribution is indeed characterized by a counterintuitive "dense-core" picture.[10] Moreover, it has been experimentally shown[11] that upon charging, the conformation changes continuously from a dense-core profile to a more smeared, evenly distributed one. This reorganization is accompanied by minor electrostatic swelling and does not depend on the generation of dendrimer. In contrast to the conformational evolution of polyelectrolyte dendrimers, much less attention has been paid to the charge influence on their dynamical response. A recent quasielastic neutron scattering (QENS) reveals an increased rapidity of the intradendrimer motion upon increasing the molecular charge.[12a] On the other hand, a Brownian dynamics (BD) simulation has also explored the dynamical features of the same system,[13] finding decreasing relaxation time of the internal pulsation for the constituent monomer with the increase of the Debye length between intradendrimer segments. It has been quantitatively demonstrated by SANS experiment,[11a] titration measurement,[14] and atomistic MD simulations[5e,11i] that upon increasing the electrostatic interaction, the intradendrimer ionic strength indeed increases progressively due to the steady counterion association with the oppositely charged amines. Therefore, upon charging, the Debye length inside a dendrimer actually decreases. Hence, the BD-predicted dynamical evolution of polyelectrolyte dendrimer is fundamentally different from the QENS results. This intrinsic disagreement clearly manifests the

Received: December 26, 2012
Published: March 12, 2013

 © 2013 American Chemical Society dx.doi.org/10.1021/ja3125959 | J. Am. Chem. Soc. 2013, 135, 5111−5117

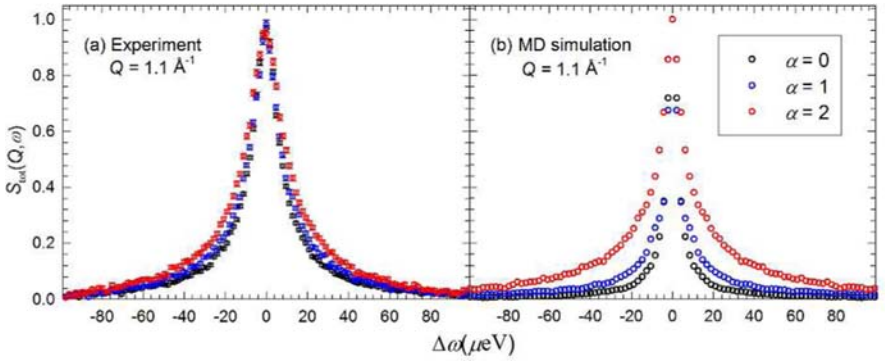

Figure 1. The normalized dynamical structure factors $S_{total}(Q,\omega)$ obtained from (a) QENS experiment after subtracting the translational center-of-mass motion of dendrimer in aqueous solutions and (b) atomistic MD simulation. In both cases, $S(Q,\omega)$ is seen to broaden upon increasing the molecular protonation. α is a parameter defined as the molar ratio of added DCl to primary amines.

ambiguity as to whether or not the approximation used in the BD simulation reflects the real intradendrimer ionic condition and therefore questions the authenticity of its predicted dynamical picture. Therefore, to date the fundamental microscopic mechanism governing the dynamical evolution of polyelectrolyte dendrimer remains elusive. This challenge provides the motivation for this study.

An essential aspect of dendrimers' structure, which differentiates them from closely packed colloids, is the accessibility of their molecular interior to the surrounding smaller solvent molecules. Our recent study, combining CVSANS experiment[11g] and atomistic MD simulation,[11h] quantitatively reveals a significant charge-induced intradendrimer hydration and clearly demonstrates the crucial role the invasive water plays in determining the dendrimer conformation. From a microscopic perspective, it is intriguing to explore the impact of invasive water on the dynamical behavior of polyelectrolyte dendrimers as a function of molecular charge.

In the present work, we conduct a coordinated study of polyelectrolyte dendrimers using atomistic MD simulation and QENS measurement, which operate at comparable length and time scales. Via a direct comparison of the computational and experimental dynamical correlation functions, we probe the microscopic mechanism governing the dynamical features of the polyelectrolyte dendrimer that is not accessible by the coarse-grained BD simulation, in which the effect of invasive water is incorporated via the hydrodynamic interactions (HI). From our fundamental consideration, we investigate the evolution of local bonding formed between the invasive water and the hydrocarbon component of dendrimer at different levels of molecular charge. A strong correlation between the developing water−dendrimer interaction and the enhancing dendrimer local dynamics is clearly demonstrated. We therefore conclude that invasive water accelerates the dendrimer dynamics, as observed by experiment.

2. SIMULATION AND EXPERIMENT

Amber[15] software was used to calculate the dynamical properties of a generation 5 (G5) PAMAM dendrimer as a function of molecular charge including an explicit solvent and chloride as the counterion. The simulation input file of G5 PAMAM dendrimer was constructed following a procedure detailed in our previous report.[11h,i] Different pH conditions of different G5 PAMAM dendrimer were represented by the different levels of amino protonation, which is represented by an acidity scale factor α defined as the ratio of the molar concentration of proton to the molar concentration of primary amines in this report. The atomic partial charges were calculated using the AM1/BCC method, and various interatomic interactions are simulated by the General Amber Force Field (GAFF). Energy minimization was applied first to the input structure to exclude an unrealistically excessive interaction energy resulting from abnormal distances between neighboring atoms. This was followed by simulated annealing for the sake of accelerating the simulation. Chloride anions were incorporated stoichiometrically to maintain the overall charge neutrality for charged dendrimer with different levels of molecular charge. The system was solvated by TIP3P water[16] in a cubic simulation box to ensure there are at least 10 Å between the outmost molecular periphery of G5 dendrimer and the boundary of the simulation box. Temperature and pressure were maintained at 300 K and 1 bar through applying Langevin dynamics and isothermal−isobaric (NPT) ensemble. The cutoff distance for force evaluation was chosen to be 10 Å. Each simulation case was conducted for at least 10 ns, and the trajectories for the last 5 ns were used for the structural and dynamical analysis presented in the next section. The simulation was carried out at the Oak Ridge Institutional Cluster (OIC) of Spallation Neutron Source (SNS), Oak Ridge National Laboratory (ORNL).

To determine the validity of the simulations, we benchmark the scattering functions obtained computationally against those from QENS measurement (Figure 1). After subtracting the contribution from translational center-of-mass motion of dendrimer and bulk D_2O background from the measured QENS spectra,[12] the normalized dynamical structure factor $S(Q,\omega)$, which represents the intradendrimer dynamics of fully protonated G5 PAMAM dendrimers, is given in Figure 1a. With the incorporation of instrumental resolution and capability of capturing dynamical relaxation only after several picoseconds (ps) to account for the limited energy transfer range accessible in the experiment, the corresponding computational counterpart calculated from MD equilibrium trajectories is presented in Figure 1b. The comparison is made at wavevector $Q = 1.1$ Å^{-1} and energy transfer ω ranging within ± 100 μeV. Despite their perceivable quantitative deviations, the experimental and computational scattering functions are indeed in fair qualitative agreement with each other. Both experimental and computational $S(Q,\omega)$ unambiguously demonstrate an enhancement in intradendrimer dynamics upon increasing the molecular charge. This dynamical enhancement from both approaches is universal to other Q values.

3. RESULTS AND DISCUSSION

Having seen that MD simulations produce trends consistent with the experimentally measured $S(Q,\omega)$, one can examine the equilibrium trajectories to investigate the mechanism leading to the dynamical enhancement. The intermediate scattering function $S(Q,\tau)$, the Fourier transformation of the dynamical structure factor, illustrates dynamical relaxation in the time domain. In this representation, the enhanced dynamics is now manifested by a faster time-decay. Compartmentalization of normalized total intermediate scattering function (Figure 2a)

dx.doi.org/10.1021/ja3125959 | J. Am. Chem. Soc. 2013, 135, 5111−5117

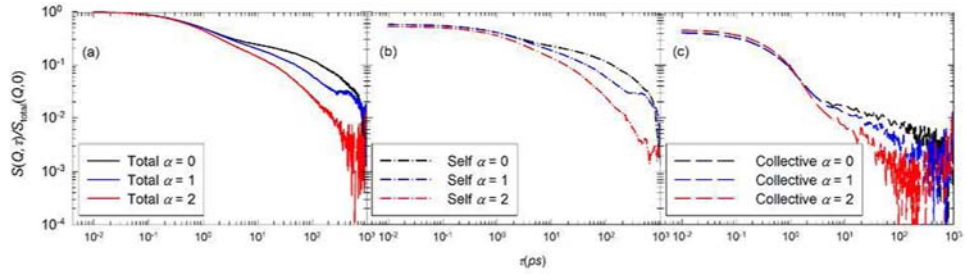

Figure 2. The MD-calculated normalized intermediate scattering functions $S(Q,\tau)/S_{total}(Q,0)$ of fully protonated G5 PAMAM dendrimer as a function of α at Q = 1.1 Å^{-1}. Their self- and collective components are given in (b) and (c), respectively.

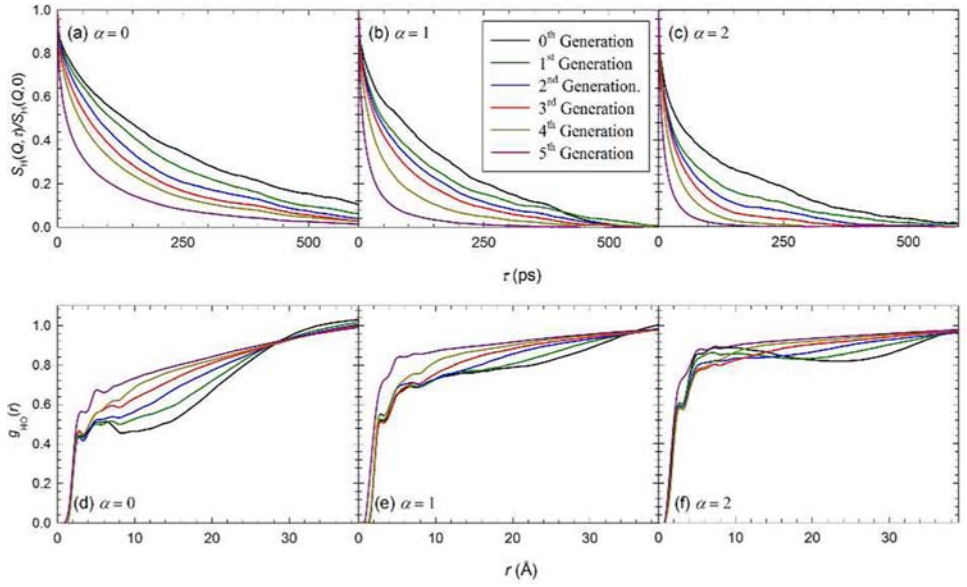

Figure 3. (a–c) The normalized $S_{inc}(Q,\tau)/S(Q,0)$ (Q = 1.1 Å^{-1}) of the protonated components of a dendrimer as a function of molecular charge and intramolecular spatial location specified by generational layer. (d–f) The partial pair distribution function $g_{HO}(r)$ between hydrogen atoms presenting in different generational layers of dendrimer and oxygen atoms of surrounding water molecules at three different levels of molecular charge.

into contributions from self-motion (Figure 2b) and collective motion (Figure 2c) clearly suggests the domination of the former part in the experimentally accessible microscopic time region (τ > 1 ps).

Furthermore, judging from the exceedingly large incoherent scattering cross section and large population of ^{1}H in G5 dendrimer, the self-motion part can be reasonably attributed to the self-motion of constituent protons. Therefore, it can be unambiguously concluded that the majority of QENS measured intensity as well as the observed dynamical enhancement, triggered by increasing molecular charge, originate from the dynamical response of ^{1}H in dendrimer. The atomistic simulations not only provide a unified basis for interpreting the measurements, they also permit one to assess the dynamical characteristics of dendrimer that are not accessible experimentally. Upon increasing the molecular charge, a steady enhancement in the collective dynamics of the hydrocarbon components of dendrimer, which is masked experimentally due to the domination of the self-motion part, is discernibly revealed by MD trajectory analysis.

Atomistic simulation allows us to seek the microscopic interpretation of this enhanced intradendrimer dynamics. First, it is instructive to note that, due to the backfolding effect,[9,10] each residual component located in a given generational layer may experience a different local environment even though they are compositionally identical. The individual dynamics could therefore be different at any given instance. However, upon averaging over sufficiently long time, the system equilibrates, and statistically each constituent residual component located in the same generational layer is dynamically similar. This approximation allows us to conveniently accelerate the data analysis and enhance the data statistics reliably. Figure 3a–c presents the resulting normalized, self-intermediate scattering functions of ^{1}H in different generational layers of G5 dendrimer. At any given Q and α, the dynamics is seen to increase closer to the molecular periphery. Moreover, consistent with the dynamical response presented in Figure 2, the relaxation time decreases considerably upon increasing the molecular charge from α = 0 to 2 for any protonated component located at the same generational layer. It is important to note that the observed charged-dependent dynamics and the varying intramolecular hydration level are strongly correlated. In Figure 3d–f, we present the partial pair distribution function $g_{HO}(r)$ between hydrogen atoms and oxygen atoms of surrounding water molecules as a function of the generational layer. Because of the effect of steric hindrance, hydrogen atoms located in inner generational layers are surrounded by fewer water molecules. As indicated by the

dx.doi.org/10.1021/ja3125959 | J. Am. Chem. Soc. 2013, 135, 5111–5117

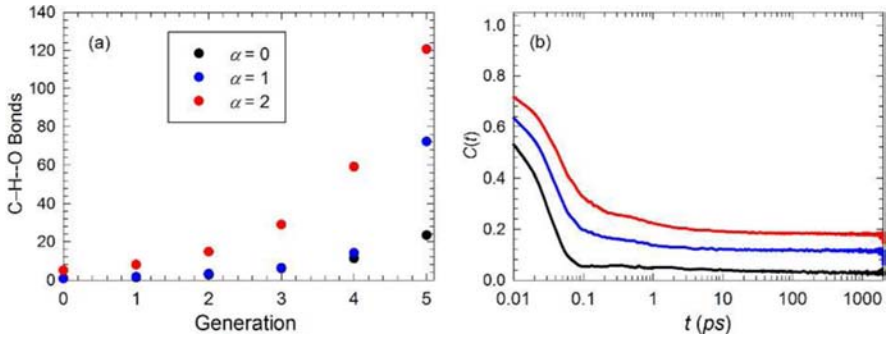

Figure 4. (a) Average population of C−H--O bonds between invasive water and constituent hydrogen of G5 dendrimer as a function of generational layers and molecular charge. (b) Relaxation of C−H--O bonds through $C(t)$ as a function of molecular charge.

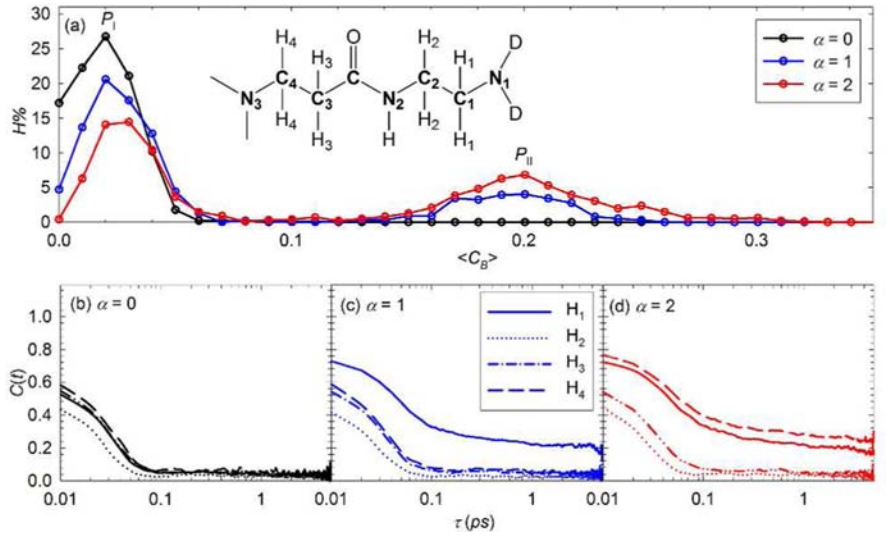

Figure 5. (a) The percentage distribution of ^{1}H of the fifth generational layer of dendrimer as a function of C−H--O bonding probability obtained from the trajectory analysis of 500 time frames (500 ps). Upon increasing the molecular charge, a bimodal distribution is evolved. The inset gives the schematic representation of fifth generational layer of G5 PAMAM dendrimer. (b−d) Relaxation of C−H--O bonds for ^{1}H at different locations of fifth generational layer and its evolution as a function of molecular charge.

evolution of $g_{HO}(r)$, the increasing intradendrimer electrostatic repulsion steadily relieves the local steric crowding and creates additional space to accommodate more invasive water molecules in each progressive generational layer.

To further scrutinize the correlation between the observed dynamical enhancement and the intradendrimer hydration level, we quantify the interaction between a dendrimer and invasive water at microscopic length scales. The electrostatic bonding between the hydrocarbon components of a dendrimer and invasive water molecules provides a suitable parameter to quantify this solvent effect from the perspective of the dendrimer−water interaction. The bond is formed between an electronegative atom X including oxygen, nitrogen, and chloride, and hydrogen (^{1}H), which forms a covalent bond with another electronegative atom Y. This bonding is commonly denoted as Y−H--X.[17] From the chemical composition of a G5 PAMAM dendrimer, approximately 90% of constituent hydrogen of the dendrimer is covalently bonded with the neighboring carbon except the labile hydrogen present in the terminal primary amine. The electronegativity of carbon (2.55 based on the Pauli scale[18]) is known to be smaller than that of oxygen (3.44). Consequently, the attraction between the C−H component of a dendrimer and oxygen atoms of water is therefore weaker than regular hydrogen bonding. This interaction, which is neither strictly a covalent bond nor an H-bond, is referred as C−H--O bond. Like any other electrostatic interaction, the relative distance between the constituent atoms and geometrical orientation is crucial in identifying its formation. To identify this C−H--O interaction in the present system, we adopt the well-accepted geometrical criteria for identifying hydrogen bonding. In our definition, one C−H--O bond is formed when the following three conditions are satisfied:[19] (I) The distance between hydrogen atom attached to carbon in the dendrimer and a water oxygen atom is less than 2.45 Å. (II) The distance between a dendrimer carbon atom and the water's oxygen atom is less than 3.6 Å. (III) The angle defined by HCO is less than 30°.

Figure 4a presents the average number of C−H--O bonds forming in each generational dendrimer layer as a function of molecular charge. Consistent with the evolution of the hydration level presented in Figure 3d−f, the number of C−H--O bonds indeed increases upon increasing α. This calculation shows a direct interaction between the dendrimer and invasive water in a quantitative manner. The origin of this enhancing water-mediated interaction is due to the increasing intradendrimer Coulomb repulsion, which outwardly relocates the terminal amines, residing in the molecular interior in the noncharged state, and creates the available water accessible

dx.doi.org/10.1021/ja3125959 | J. Am. Chem. Soc. 2013, 135, 5111−5117

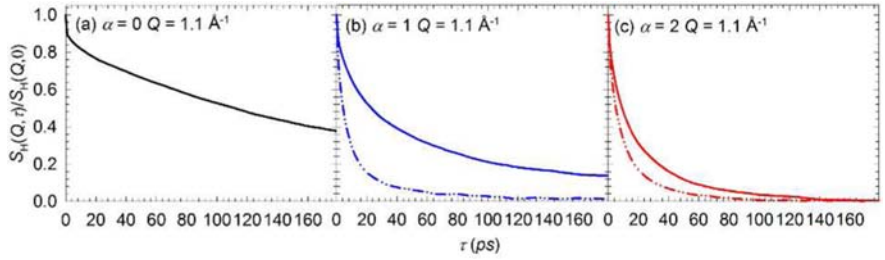

Figure 6. The normalized self-intermediate scattering function $S_H(Q,\tau)/S_H(Q,0)$ of ^{1}H as a function of molecular charge ((a) $\alpha = 0$, (b) $\alpha = 1$, and (c) $\alpha = 2$). In (b) and (c), the constituent ^{1}H atoms of charged dendrimers are partitioned into two groups based on the C−H--O bonds statistics presented in Figure 5a. Solid lines and dash−dotted lines represent, respectively, the $S_H(Q,\tau)/S_H(Q,0)$ of ^{1}H belonging to groups P_I and P_{II} as shown in Figure 5.

space for the formation of C−H--O bonds. To further investigate the lifetime of the water−dendrimer interaction, we adapt the hydrogen-bond population operator, $H_i(t)$,[20] proposed by Chandler et al. as a bookkeeping parameter to register the C−H--O bonding status in the dendrimer. On the basis of this definition, $H_i(t)$ is equal to one if the ith hydrogen bonded to carbon forms a C−H--O bond with any oxygen of invasive water at instant t. $H_i(t)$ is equal to zero when no C−H--O bond is formed between the ith hydrogen and surrounding water. The relaxation of C−H--O bonding for ^{1}H in the dendrimer can therefore be defined by the following expression:

$$C(t) = \frac{\langle H_i(t)H_i(0)\rangle}{\langle H_i(0)\rangle} \quad (1)$$

where the angular bracket represents the ensemble average. The calculated $C(t)$ given in Figure 4b is seen to be characterized by a two-step relaxation and saturation. Trajectory analysis suggests the first steep decay, within the time interval less than 0.1 ps, indeed manifests the fast reorientation of localized water. Therefore, it characterizes the averaged bonding lifetime between ^{1}H and oxygen atoms belonging to a specific water molecule. This fast decay is followed by a slow relaxation, which reaches its plateau around 10 ps. Despite the short bonding lifetime between ^{1}H and any given water molecule, it is the incessant breaking-associating process that renders the long-lived C−H--O bonding between any given ^{1}H and many different water molecules. The evolution of a plateau value suggests that the hydrocarbon component of dendrimer with higher level of molecular charge indeed has a higher probability of retaining the formation of C−H--O bonding by paring with various water molecule. Consequently, with increased charge, the dendrimer relaxation, as reflected by the QENS, is affected through coupling with an increased number of pairing water molecules that are characterized by much faster dynamics.

To provide further support to the above interpretation, the dependence of the relaxation of the hydrocarbon component of a dendrimer on the C−H--O bonding number is estimated from the MD trajectory analysis. The total number of the C−H--O bonds, $\sum_{t=0}^{500ps} H_i(t)$, forming between ith ^{1}H atom in the fifth generational layer of a dendrimer and its surrounding water molecules is registered within the 500 frames of MD trajectories corresponding to the time interval of 500 ps. The distribution, denoted as $\langle C_B\rangle$, of frame-averaged C−H--O bonds number, $(1/500)\sum_{t=0}^{500ps} H_i(t)$, is presented in Figure 5a.

At the neutral state ($\alpha = 0$, black line), only moderate connectivity between ^{1}H and invasive water is developed because the majority of ^{1}H is distributed within the range of $\langle C_B\rangle$ less than 0.1. Upon increasing the molecular charge, a bimodal distribution of $\langle C_B\rangle$ is developed (blue line for $\alpha = 1$ and red line for $\alpha = 2$) as indicated by the diminishing peak (denoted as P_I) centering at 0.05 and the additional one (P_{II}) centering at 0.2 with enhancing height. This finding is surprising because it is contrary to the intuitive expectation of a continuous possibility distribution with an evolving mean. Moreover, it is important to point out that this charge-induced bimodal distribution is also observed in ^{1}H belonging to second, third, and fourth generational layers upon increasing the molecular charge. Whether it happens for ^{1}H belonging to zeroth and first generational layers cannot be conclusively determined due to the limitation of poor statistics.

We attribute the cause of this observation to the increasing intradendrimer electrostatic interaction. To demonstrate this point, we further categorize the ^{1}H according to their spatial location in the fifth generational layer whose schematic representation is given in the inset of Figure 5a. The corresponding $C(t)$ values are calculated and given in Figure 5b−d as a function of molecular charge. In the noncharged neutral state ($\alpha = 0$, Figure 5b), the relaxation of C−H--O essentially shows no dependence on the spatial location of ^{1}H. When α is increased to 1, the relaxation of C−H--O bond forming between the type one of ^{1}H (denoted as H_1) and invasive water is seen to significantly slow (blue solid curve of Figure 5c). This dynamical stabilization could be partially caused by the protonation of primary amines (denoted by nitrogen atom N_1), which create the additional local space. This interesting dynamical feature is again illuminated by the calculated $C(t)$ presented in Figure 5d when dendrimer is fully charged ($\alpha = 2$). While the $C(t)$ values corresponding to H_2 and H_3 (dotted curve and dashed−dotted curve, respectively) are independent of α, the relaxation of C−H--O involving H_4 (dashed curve), next to the charged tertiary amines (denoted by nitrogen atom N_3) at $\alpha = 2$, exhibits the same dynamical characteristics as that of H_1 at $\alpha = 1$ and $\alpha = 2$.

Figure 5 illustrates two important points. First, the integrated number of ^{1}H that contributes to the second peak, that is, P_{II}, can be obtained. For both cases of $\alpha = 1$ and 2, the values are found to be 250 and 470, respectively, which are in good quantitative agreement with the numbers of ^{1}H in the $-CH_2-$ groups directly bonded with charged amines (256 for $\alpha = 1$ and 512 for $\alpha = 2$, respectively). Second, a close link exists between the plateau value of $C(t)$ and the peak position of ^{1}H distribution presented in Figure 5a. For $\alpha = 0$, $C(t = 5$ ps) for all four types of ^{1}H is found to be around 0.05, which is identical to the peak value of P_I. For $\alpha = 1$, the value of $C(t = 5$

dx.doi.org/10.1021/ja3125959 | J. Am. Chem. Soc. 2013, 135, 5111−5117

ps) of H_1 (blue solid curve of Figure 5c) is 0.2 and is identical to the peak value of P_{II}, while the values of $C(t = 5$ ps) for the rest of ^{1}H remain invariant and again identical to the peak value of P_I. Upon increasing α to 2, the value of $C(t = 5$ ps) of H_4 (red dashed curve of Figure 5d) is found to be 0.25, which is again identical to the peak position corresponding to the additional bump of the red curve of Figure 5a. These findings suggest self-consistency in two independent analysis approaches.

The bimodal distribution of C−H--O bond statistics shown in Figure 5 can be conveniently used as a criteria to categorize ^{1}H present in the fifth generational dendrimer layer. The normalized self-intermediate scattering functions $S_H(Q,\tau)/S_H(Q,0)$ corresponding to ^{1}H belonging to the two different groups, P_I and P_{II}, are calculated to reveal the dependence of the relaxation of ^{1}H on their interaction with surrounding water molecules (Figures 6). At three calculated levels of molecular charge, it clearly shows that the stronger interaction between a dendrimer and invasive water, via forming more C−H--O bonds with longer lifetime, indeed leads to faster relaxation of hydrogen present in the pairing hydrocarbon component. This observation again demonstrates the correlation between the local dynamics of the dendrimer and the invasive water from a complementary perspective. Moreover, it is instructive to comment that while there may not be a single mechanism responsible for the essential dynamical features of polyelectrolyte dendrimer, their dependence on the water−dendrimer interaction at a microscopic level is clearly revealed in this coordinated study. It is our opinion that this highly localized, discrete interaction within the confined intradendrimer interior cannot be satisfactorily described by the BD simulation in which the solvent effect is treated in the mean-field approximation.

4. CONCLUSIONS

In this Article, we investigate the local segmental dynamics of G5 PAMAM dendrimers dissolved in D_2O and its dependence on molecular charge. The atomistic MD simulation, in which water molecules are incorporated explicitly, renders a dynamical picture that is in an agreement with that obtained from QENS experiments. Thus this work presents a valid computational model to describe qualitatively the dynamical response of the polyelectrolyte dendrimer under the influence of charge. We demonstrate a strong correlation between the enhancement of both self- and collective intradendrimer dynamics and the increase in the local hydration level. The interaction between the hydrocarbon components of the dendrimer and invasive water is quantified by the formation of C−H--O bonds based on a geometric definition. We find that the C−H--O bond provides a mechanism for coupling the local dynamics of the hydrocarbon component of the dendrimer to the much faster dynamics of the invasive water within the length scale of the experimental observation. While whether the invasive water is the only driving mechanism responsible for the structural relaxation of polyelectrolyte dendrimer remains a matter for scientific debate and investigation, this report unambiguously reveals their close correlation. Moreover, the success of using atomistic MD simulation in describing the experimentally observed dynamical response of a polyelectrolyte dendrimer may be extended to the theoretical study of dynamics of general polyelectrolytes systems. In many theoretical investigations, the solvent effect is considered via mean field treatment.[21,22] The influence of the discreteness of local water−polymer bonding on the predicted dynamical picture is unknown, and this is therefore a promising area of fruitful future research.

AUTHOR INFORMATION

Corresponding Author

yunliu@nist.gov; chenw@ornl.gov

Notes

The authors declare no competing financial interest.

ACKNOWLEDGMENTS

Research presented in this work is supported by the U.S. Department of Energy, Basic Energy Sciences, Materials Sciences and Energy Division. The computation was carried out at the ORNL Institutional Cluster, which is sponsored at Oak Ridge National Laboratory by the Scientific User Facilities Division, Office of Basic Energy Sciences, U.S. Department of Energy. The QENS experiment on the backscattering neutron spectrometer (BASIS) at Oak Ridge National Laboratory's Spallation Neutron Source is supported by the Scientific User Facilities Division, Office of Basic Energy Sciences, U.S. Department of Energy. The QENS experiment on the disk chopper spectrometer (DCS) at NIST Center for Neutron Research utilized facilities supported in part by the National Science Foundation under Agreement No. DMR-0944772. We are also much indebted to Professors Yang Zhang and Feng Ding and Doctor Christopher E. Bertrand for helpful discussions.

REFERENCES

(1) (a) Ballauff, M.; Likos, C. N. *Angew. Chem., Int. Ed.* **2004**, *43*, 2998−3020. (b) Likos, C. N.; Ballauff, M. *Top. Curr. Chem.* **2005**, *245*, 239−252. (c) Likos, C. N. *Soft Matter* **2006**, *2*, 478−498. (d) Tian, W.; Ma, Y. *Chem. Soc. Rev.* **2013**, *2*, 705−727.

(2) Lee, C. C.; MacKay, J. A.; Fréchet, J. M. J.; Szoka, F. C. *Nat. Biotechnol.* **2005**, *23*, 1517−1526.

(3) Astruc, D.; Boisselier, E.; Omelas, C. *Chem. Rev.* **2010**, *110*, 1857−1959.

(4) (a) Govorun, E. N.; Zeldovich, K. B.; Khokhlov, A. R. *Macromol. Theory Simul.* **2003**, *12*, 705−713. (b) Lewis, T.; Pryamitsyn, V.; Ganesan, V. *J. Chem. Phys.* **2011**, *135*, 204902-1−204902-16.

(5) (a) Giupponi, G.; Martin, D.; Buzza, A.; Adolf, D. B. *Macromolecules* **2007**, *40*, 5959−5965. (b) Lee, I.; Athey, B. D.; Wetzel, A. W.; Meixner, W.; Baker, J. R. *Macromolecules* **2002**, *35*, 4510−4520. (c) Carbone, P.; Müller-Plathe, F. *Soft Matter* **2009**, *5*, 2638−2647. (d) Freire, J. J. *Soft Matter* **2008**, *4*, 2139−2143. (e) Maiti, P. K.; Çağin, T.; Lin, S.-T.; Goddard, W. A. *Macromolecules* **2005**, *38*, 979−991. Maiti, P. K.; Goddard, W. A. *J. Phys. Chem. B* **2006**, *110*, 25628−25632. Liu, Y.; Bryantsev, V. S.; Maiti, P. K.; Bagchi, B. *J. Chem. Phys.* **2009**, *131*, 214901-1−214901-7. Diallo, M. S.; Goddard, W. A. *J. Am. Chem. Soc.* **2009**, *131*, 2798−2799. (f) Karatasos, K. *Macromolecules* **2008**, *41*, 1025−1033. Tanis, I.; Karatasos, K. *Phys. Chem. Chem. Phys.* **2009**, *11*, 10017−10028. Karatasos, K.; Krystallis, M. *J. Chem. Phys.* **2009**, *130*, 114903-1−114903-11. Karatasos, K.; Tanis, I. *Macromolecules* **2011**, *44*, 6605−6614. (g) Majtyka, M.; Kłos, J. S. *J. Phys.: Condens. Matter* **2006**, *9*, 2284−2292. Majtyka, M.; Kłos, J. S. *Phys. Chem. Chem. Phys.* **2007**, *18*, 3581−3589. Kłos, J. S.; Sommer, J.-U. *Macromolecules* **2010**, *43*, 4418−4427. Kłos, J. S.; Sommer, J.-U. *Macromolecules* **2010**, *43*, 10659−10667. (h) Suman, B.; Kumar, S. *J. Phys. Chem. B* **2007**, *111*, 8728−8739. (i) Lee, H.; Baker, J. R.; Larson, R. G. *J. Phys. Chem. B* **2006**, *110*, 4014−4019. Lee, H.; Larson, R. G. *J. Phys. Chem. B* **2006**, *110*, 18204−18211. (j) Likos, C. N.; Blaak, R.; Wynveen, A. *J. Phys.: Condens. Matter* **2008**, *20*, 494221-1−494221-10. Blaak, R.; Lehmann, S.; Likos, C. N. *Macromolecules* **2008**, *41*, 4452−4458. Huißmann, S.; Wynveen, A.; Likos, C. N.; Blaak, R. *J. Phys.: Condens. Matter* **2010**, *20*, 232101-1−232101-8. Huißmann, S.; Likos, C. N.; Blaak, R. *Soft Matter* **2011**, *7*, 8419−8427. Huißmann, S.; Likos,

C. N.; Blaak, R. *Macromolecules* **2012**, *45*, 2562−2569. (k) Lyulin, S. V.; Evers, L. J.; van der Schoot, P.; Darinskii, A. A.; Lyulin, A. V.; Michels, M. A. J. *Macromolecules* **2004**, *37*, 3049−3063. Gurtovenko, A. A.; Lyulin, S. V.; Karttunen, M.; Vattulainen, I. *J. Chem. Phys.* **2006**, *124*, 094904-1−094904-8. (l) Tian, W.; Ma, Y. *J. Phys. Chem. B* **2009**, *113*, 13161−13170. Tian, W.; Ma, Y. *Soft Matter* **2010**, *6*, 1308−1316. (m) Welch, P.; Muthukumar, M. *Macromolecules* **1998**, *31*, 5892−5897. (n) Paulo, P. M. R.; Lopes, J. N. C.; Costa, S. M. B. *J. Phys. Chem. B* **2007**, *111*, 10651−10664. (o) Terao, T.; Nakayama, T. *Macromolecules* **2004**, *37*, 3049−3063. Terao, T. *Mol. Phys.* **2006**, *104*, 2507−2513.

(6) (a) Nisato, G.; Ivkov, R.; Amis, E. J. *Macromolecules* **1999**, *32*, 5895−5900. Nisato, G.; Ivkov, R.; Amis, E. J. *Macromolecules* **2000**, *33*, 4172−4176. (b) Feng, X.; Taton, D.; Borsali, R.; Chaikof, E. L.; Gnanou, Y. *J. Am. Chem. Soc.* **2006**, *128*, 11551−11562. (c) Niu, Y.; Sun, L.; Crooks, M. *Macromolecules* **2003**, *36*, 5725−5731. (d) Wang, X.; Imae, T. *J. Am. Chem. Soc.* **2004**, *126*, 13204−13205. (e) Ohshima, A.; Konishi, T.; Yamanaka, J.; Ise, N. *Phys. Rev. E* **2001**, *64*, 051808-1−051808-9. (f) Kabanov, V. A.; Zezin, A. B.; Rogacheva, V. B.; Gulyaeva, Zh. G.; Zansochova, M. F.; Joosten, J. G. H.; Brackman, J. *Macromolecules* **1999**, *32*, 5895−5900. (g) Huang, Q. R.; Dubin, P. L.; Lal, J.; Moorefield, C. N.; Newkome, G. R. *Langmuir* **2005**, *21*, 2737−2742. (h) Lombardo, D. *Langmuir* **2009**, *25*, 3271−3275. (i) Micali, N.; Monsu, L.; Romeo, A.; Lombardo, D.; Lesieur, P.; Mallamace, F. *Phys. Rev. E* **1998**, *58*, 6229−6235. (i) Ramzi, A.; Scherrenberg, R.; Brackman, J.; Joosten, J.; Mortensen, K. *Macromolecules* **1998**, *31*, 1621−1626. Ramzi, A.; Scherrenberg, R.; Joosten, J.; Lemstra, P.; Mortensen, K. *Macromolecules* **2002**, *35*, 827−833. (k) Rietveld, I. B.; Bouwman, W. G.; Baars, M. W. P. L.; Heenan, R. K. *Macromolecules* **2001**, *34*, 8380−8383. (l) Chen, W.; Tomalia, D. A.; Thomas, J. L. *Macromolecules* **2000**, *33*, 9169−9172.

(7) Rosenfeldt, S.; Dingenouts, N.; Ballauff, M.; Werner, N.; Vögtle, F.; Lindner, P. *Macromolecules* **2002**, *35*, 8098−8105.

(8) Aumanen, J.; Kesti, T.; Sundström, V.; Teobaldi, G.; Zerbetto, F.; Werner, N.; Richardt, G.; van Heyst, J.; Vögtle, F.; Korppi-Tommola, J. *J. Phys. Chem. B* **2010**, *110*, 1548−1558.

(9) Zook, T. C.; Pickett, G. T. *Phys. Rev. Lett.* **2003**, *90*, 015502-1−015502-4.

(10) Lescanec, R. L.; Muthukumar, M. *Macromolecules* **1990**, *23*, 2280−2288.

(11) (a) Chen, W.-R.; Porcar, L.; Liu, Y.; Butler, P. D.; Magid, L. J. *Macromolecules* **2007**, *40*, 5887−5898. (b) Li, T.; Hong, K.; Porcar, L.; Verduzco, R.; Butler, P. D.; Smith, G. S.; Liu, Y.; Chen, W.-R. *Macromolecules* **2008**, *41*, 8916−8920. (c) Porcar, L.; Liu, Y.; Verduzco, R.; Hong, K.; Butler, P. D.; Magid, L. J.; Smith, G. S.; Chen, W.-R. *J. Phys. Chem. B* **2008**, *112*, 14772−14778. (d) Porcar, L.; Hong, K.; Butler, P. D.; Herwig, K. W.; Smith, G. S.; Liu, Y.; Chen, W.-R. *J. Phys. Chem. B* **2010**, *114*, 1751−1756. (e) Liu, Y.; Porcar, L.; Hong, K.; Shew, C.-Y.; Li, X.; Liu, E.; Butler, P. D.; Herwig, K. W.; Smith, G. S.; Chen, W.-R. *J. Chem. Phys.* **2010**, *132*, 124091-1−124901-6. (f) Liu, Y.; Chen, C.-Y.; Chen, H.-L.; Hong, K.; Shew, C.-Y.; Li, X.; Liu, L.; Melnichenko, Y.; Smith, G. S.; Herwig, K. W.; Porcar, L.; Chen, W.-R. *J. Phys. Chem. Lett.* **2010**, *1*, 2020−2024. (g) Wu, B.; Li, X.; Do, C.; Kim, T.-H.; Shew, C.-Y.; Liu, Y.; Yang, J.; Hong, K.; Porcar, L.; Chen, C.-Y.; Liu, E. L.; Smith, G. S.; Herwig, K. W.; Chen, W.-R. *J. Chem. Phys.* **2011**, *135*, 144903-1−144901-9. (h) Wu, B.; Kerkeni, B.; Egami, T.; Do, C.; Liu, Y.; Wang, Y.; Porcar, L.; Hong, K.; Smith, S. C.; Liu, E. L.; Smith, G. S.; Chen, W.-R. *J. Chem. Phys.* **2012**, *136*, 144903-1−144901-9. (i) Wu, B.; Chen, W.-R.; Egami, T.; Li, X.; Liu, Y.; Wang, Y.; Do, C.; Porcar, L.; Hong, K.; Liu, L.; Smith, G. S.; Smith, S. C. *J. Chem. Phys.* **2012**, *136*, 064902-1−064902-9.

(12) (a) Li, X.; Zamponi, M.; Hong, K.; Porcar, L.; Shew, C.-Y.; Jenkins, T.; Liu, E.; Smith, G. S.; Herwig, K. W.; Liu, Y.; Chen, W.-R. *Soft Matter* **2011**, *7*, 618−622. (b) Mamontov, E.; Herwig, K. W. *Rev. Sci. Instrum.* **2011**, *82*, 085109-1−085109-10. (c) Copley, J. R. D.; Cook, J. C. *Chem. Phys.* **2003**, *292*, 477−485.

(13) Lyulin, S. V.; Darinskii, A. A.; Lyulin, A. V.; Michels, M. A. J. *Macromolecules* **2004**, *37*, 4676−4685.

(14) Niu, Y.; Sun, L.; Crooks, R. M. *Macromolecules* **2003**, *36*, 5725−5731.

(15) In their own activities as scientific institutions, NIST and ORNL use many different materials, products, types of equipment, and services. However, NIST and ORNL do not approve, recommend, or endorse any product or proprietary material.

(16) Jorgensen, W. L. *J. Am. Chem. Soc.* **1981**, *103*, 335−340.

(17) Israelachvili, J. N. *Intermolecular and Surface Forces*, 3rd ed.; Academic Press: Amsterdam, 2011.

(18) Pauling, L. *J. Am. Chem. Soc.* **1932**, *54*, 3570−3582.

(19) Marti, J.; Pardo, J. A.; Guardia, E. *J. Chem. Phys.* **1996**, *105*, 639−649.

(20) Luzar, A.; Chandler, D. *Nature* **1996**, *379*, 55−57.

(21) Muthukumar, M. *Adv. Chem. Phys.* **2005**, *131*, 1−60.

(22) Dobrynin, D. A.; Rubinstein, M. *Prog. Polym. Sci.* **2005**, *30*, 1049−1118.